Fundamental J. Modern Physics, Vol. 1, Issue 1, 2011, Pages 1-22
Published online: June 2, 2011

TAMING OF DIVERGENCES IN A UNITARY MODEL OF MASSIVE TENSORS, VECTORS, SCALARS AND SPINORS

E. MENDELS

Schenkkade 221
The Hague, 2595 AT, The Netherlands
e-mail: emendels@zonnet.nl

Abstract

We consider a unitary model of a massive tensor and vector field interacting with scalars and spinors. It is shown that the scattering matrix - not each Feynman diagram apart - can be made finite by appropriate relations of the coupling constants, order by order in perturbation.

1. Introduction

In a recently published paper [1], we considered a model of a massive vector field W^μ interacting with a spinor field ψ and a self interacting scalar field φ according to the Lagrangian

$$L = L_{\text{free}} + \lambda_{FV}\overline{\psi}\gamma_\mu\psi W^\mu + \lambda_{VS}W_\mu W^\mu\varphi + \lambda'_S\varphi^3 + \lambda_S\varphi^4, \tag{1.1}$$

where the unitary propagator of a vector field with mass m_V,

$$\sum_{\lambda=1}^{n-1} \frac{e_\lambda^\mu e_\lambda^\nu}{(k^2 + {m_V}^2)} = \frac{k^\mu k^\nu + {m_V}^2 g^{\mu\nu}}{{m_V}^2(k^2 + {m_V}^2)}, \tag{1.2}$$

was used. The summation in the left hand side (l.h.s.) is over transversal eigenvectors e_λ^μ only, while longitudinal eigenvectors k^μ are absent, so that their negative metric

Keywords and phrases: Feynman diagrams, renormalization, taming of divergences, tensor fields.
Received December 27, 2010

need not be compensated by ghost particles. In this way, unitarity is built in from the very beginning.

The vertices of Figure 1 are represented in the Feynman diagrams of this model.

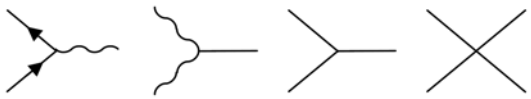

Figure 1. Vertices of Lagrangian (1.1).

Because of the momenta in the numerator of the vector propagator, the divergences of Feynman diagrams are stronger than in the corresponding scalar case. Compensation by counter terms would lead to new and stronger divergences, i.e., the theory seems to be non-renormalizable. For this reason, spontaneously broken gauge theories have been introduced [2-5] to describe massive vector bosons.

Figure 2. Vector-vector and vector-scalar vertices, excluded from (1.1).

A second formalism to describe massive vector bosons has been presented in [1], where all masses are introduced directly into the Lagrangian so that there is global, but no local gauge symmetry. Instead, interactions between two vectors and two scalars, as well as three-vector and four-vector interactions, are excluded. These have to be described indirectly, by means of an intermediate scalar field or via a spinor loop.

Due to momentum conservation at each vertex, many momenta in the numerator are transformed into harmless mass dependent factors. This entails a cancellation of divergences, which has been transparently shown, to all orders of perturbation, by using configuration space parameters. Thus, the degree of divergence of many diagrams of spinning fields is smaller than expected by simple counting of powers in momentum space.

It also has been shown that the divergences of Feynman diagrams with two and three external lines and of those with four external scalars become finite by the introduction of counter terms. Diagrams with four external vectors and those with two external vectors and scalars cannot be renormalized by counter terms.

However, it has been shown that the degree of divergence of the latter diagrams is logarithmic in lowest order and, due to the restriction of the possible interactions, it does not increase in higher orders. In consequence, the divergence of diagrams with four external lines is at most logarithmic to all orders of perturbation and, therefore, it is possible to construct a finite scattering matrix by imposing appropriate relations on the coupling constants. In this sense, the formalism is renormalizable.

Thus, a narrow escape from non-renormalizibility is obtained in four steps: (a) restriction of the possible interactions, (b) a less severe divergence criterion in the case of spinning fields, (c) relations of coupling constants and (d) extension of the concept "renormalizibility", it is the scattering matrix that has to become finite, not necessarily, by counter terms renormalized, the Feynman diagrams.

In this paper, the formalism is extended by adding a massive tensor field $W_{\mu\nu}$ to (1.1) and we consider the Lagrangian

$$L = L_{\text{free}} + \lambda_{FV}\overline{\psi}\gamma_\mu\psi W^\mu + \lambda_{FT}\overline{\psi}\gamma_\mu\gamma_\nu\psi W^{\mu\nu} + \lambda_{VS}W_\mu W^\mu\varphi + \lambda_{TS}W_{\mu\nu}W^{\mu\nu}\varphi + \lambda'_S\varphi^3 + \lambda_S\varphi^4 \tag{1.3}$$

with

$$L_{\text{free}} = \tfrac{1}{2}\partial_\rho W_{\mu\nu}\partial^\rho W^{\mu\nu} - \tfrac{1}{2}m_T{}^2W_{\mu\nu}W^{\mu\nu} - \tfrac{1}{2}\partial_\mu W_\nu\partial^\mu W^\nu + \tfrac{1}{2}m_V{}^2W_\mu W^\mu + \overline{\psi}(i\gamma^\mu\partial_\mu - m_F)\psi + \tfrac{1}{2}\partial_\mu\varphi\partial^\mu\varphi - \tfrac{1}{2}m_S{}^2\varphi^2. \tag{1.4}$$

It differs from (1.1) by a tensor-spinor and a tensor-scalar interaction and it leads to the vertices of Figure 1 and, in addition, to those of Figure 3. It is invariant under global Lorentz transformations, but not under local ones.

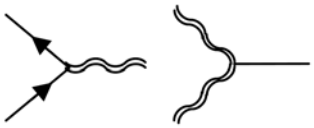

Figure 3. Additional tensor vertices of Lagrangian (1.3).

The propagator of the mass m_T tensor field is represented by a double wave line corresponding to the expression

$$\sum_{\lambda,\lambda'=1,1}^{n-1,n-1} \frac{(e_\lambda^\mu e_{\lambda'}^\nu)(e_\lambda^\rho e_{\lambda'}^\sigma)}{(k^2 + {m_T}^2)}$$

$$= \frac{(k^\mu k^\nu k^\rho k^\sigma + {m_T}^2 k^\mu k^\rho g^{\nu\sigma} + {m_T}^2 k^\mu k^\sigma g^{\nu\rho} + {m_T}^4 g^{\mu\rho} g^{\nu\sigma})}{{m_T}^4 (k^2 + {m_T}^2)}. \tag{1.5}$$

The summation in the left hand side is over double transversal tensors ee' only. These satisfy the relations

$$ee' : e''k = ee' : ke'' = ee' : kk = 0, \tag{1.6}$$

with notation

$$ab : cd \equiv (a.c)(b.d), \tag{1.7}$$

so that longitudinal (kk) and half longitudinal $(ke$ or $ek)$ eigentensors of the propagator have eigenvalue 0 and no ghost fields have to be introduced to compensate for their negative metric. Thus, unitarity is guaranteed as long as only double transversal (ee') external tensors come in and go out.

To make this paper self-supporting, the method of [1] is summarized in Section 2 and the degree of divergence of the Feynman diagrams resulting from (1.1) is discussed in Section 3. In Section 4, we show that the Lagrangian (1.3), unlike Lagrangian (1.1), does not lead to a finite scattering matrix, though the formalism of [1] is applied to obtain a reduced degree of divergence.

In Section 5, we show that the Lagrangian

$$L = L_{\text{free}} + \sum_{f=1}^{g} \{\lambda_{f\,FV} \overline{\psi}_f \gamma_\mu \psi_f W^\mu + \lambda_{f\,FT} \overline{\psi}_f \gamma_\mu \gamma_\nu \psi_f W^{\mu\nu}\}$$

$$+ \lambda_{VS} W_\mu W^\mu \varphi + \lambda'_S \varphi^3 + \lambda_S \varphi^4, \tag{1.8}$$

in which tensor interactions with several spinor fields, according to Figure 4, are allowed, whereas tensor-scalar interactions are excluded, does lead to a finite scattering matrix, provided that the number of participating spinor fields is at least two $(g \geq 2)$.

Figure 4. Tensor-spinor and vector-spinor vertices of Lagangian (1.8).

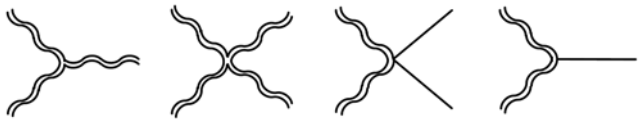

Figure 5. Tensor-tensor and tensor-scalar vertices, excluded from Lagrangian (1.8).

2. Massive Vector, Scalar and Spinor Fields

Configuration space parameters are used to show transparently the cancellation of part of the divergences. The formalism may be found in [1] and a summary is given in this section. We illustrate the method by means of the most simple scalar two-vertex diagram of Figure 6.

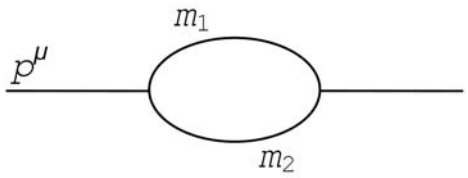

Figure 6. Two-vertex scalar diagram.

Its expression in n dimensions is

$$\int d^n k_1 d^n k_2 \frac{\delta^n(p-k_1-k_2)}{({k_1}^2+{m_1}^2)({k_2}^2+{m_2}^2)}$$

$$=\frac{(2\pi^{n/2})^2(m_1m_2)^{2b}}{(2\pi)^n}\int d^n x e^{ip.x}k_b(m_1x)k_b(m_2x). \qquad (2.1)$$

The l.h.s. is the momentum space expression, the right hand side (r.h.s.) is the configuration space expression. The functions $k_b(mx)$ of order

$$b=\tfrac{1}{2}n-1 \qquad (2.2)$$

are the Fourier transforms of the propagators. They differ by a factor $(\frac{1}{2}mx)^{-b}$ from

Hankel functions [6] with a purely imaginary argument,

$$k_b(mx) \equiv (\tfrac{1}{2}mx)^{-b} K_b(mx), \tag{2.3}$$

and satisfy the Euclidean Klein Gordon equation

$$\partial_\mu \partial^\mu k_b(mx) = m^2 k_b(mx). \tag{2.4}$$

Properties like series expansion, asymptotic behaviour, recursion relations, differential equations and splitting formulas, are found in the appendices of [1]. From the r.h.s. of (2.1), the near threshold expansion is obtained by doing angular integrations $\int d^n\hat{x}$ and radial integrations $\int dx x^{n-1}$. Dimensional regularization is introduced according to

$$\int d^n x = \int_0^{\Lambda/T} dx x^{n+2\varepsilon-1} \int d^n \hat{x}, \tag{2.5}$$

where

$$T = m_1 + m_2 - p \tag{2.6}$$

is the threshold. Term by term performance of the integrations yields a sum of 16 near threshold expansions,

$$\text{r.h.s. (2.1)} = \pi^{n/2}(m_1 m_2)^{2b}\left(\frac{\Lambda}{2T}\right)^n \sum_{q/2,\, k_1,\, k_2 = 0}^{\infty} A_0^0(q)\left(\frac{p\Lambda}{2T}\right)^q \left(\frac{m_1\Lambda}{2T}\right)^{2k_1}\left(\frac{m_2\Lambda}{2T}\right)^{2k_2}$$

$$\times \Bigg[\frac{R_b^{00}(k_1)R_b^{00}(k_2)}{(\varepsilon + n/2 + q/2 + k_1 + k_2)} + \frac{R_b^{00}(k_1)R_b^{11}(k_2)}{(\varepsilon + n/2 + q/2 + k_1 + k_2)} \ln\left(\frac{m_2\Lambda}{2T}\right)^2$$

$$- \frac{R_b^{00}(k_1)R_b^{11}(k_2)}{(\varepsilon + n/2 + q/2 + k_1 + k_2)^2} + \frac{R_b^{00}(k_1)R_b^{01}(k_2)}{(\varepsilon + n/2 - b + q/2 + k_1 + k_2)}\left(\frac{m_2\Lambda}{2T}\right)^{-2b}$$

$$+ \frac{R_b^{11}(k_1)R_b^{00}(k_2)}{(\varepsilon + n/2 + q/2 + k_1 + k_2)} \ln\left(\frac{m_1\Lambda}{2T}\right)^2 - \frac{R_b^{11}(k_1)R_b^{00}(k_2)}{(\varepsilon + n/2 + q/2 + k_1 + k_2)^2}$$

$$+ \frac{R_b^{11}(k_1)R_b^{11}(k_2)}{(\varepsilon + n/2 + q/2 + k_1 + k_2)} \ln\left(\frac{m_1\Lambda}{2T}\right)^2 \ln\left(\frac{m_2\Lambda}{2T}\right)^2$$

$$
- \frac{R_b^{11}(k_1)R_b^{11}(k_2)}{(\varepsilon + n/2 + q/2 + k_1 + k_2)^2} \ln\left(\frac{m_1\Lambda}{2T}\right)^2 - \frac{R_b^{11}(k_1)R_b^{11}(k_2)}{(\varepsilon + n/2 + q/2 + k_1 + k_2)^2} \ln\left(\frac{m_2\Lambda}{2T}\right)^2
$$

$$
+ \frac{2R_b^{11}(k_1)R_b^{11}(k_2)}{(\varepsilon + n/2 + q/2 + k_1 + k_2)^3} + \frac{R_b^{11}(k_1)R_b^{01}(k_2)}{(\varepsilon + n/2 - b + q/2 + k_1 + k_2)} \left(\frac{m_2\Lambda}{2T}\right)^{-2b} \ln\left(\frac{m_1\Lambda}{2T}\right)^2
$$

$$
- \frac{R_b^{11}(k_1)R_b^{01}(k_2)}{(\varepsilon + n/2 - b + q/2 + k_1 + k_2)^2} \left(\frac{m_2\Lambda}{2T}\right)^{-2b} + \frac{R_b^{01}(k_1)R_b^{00}(k_2)}{(\varepsilon + n/2 - b + q/2 + k_1 + k_2)} \left(\frac{m_1\Lambda}{2T}\right)^{-2b}
$$

$$
+ \frac{R_b^{01}(k_1)R_b^{11}(k_2)}{(\varepsilon + n/2 - b + q/2 + k_1 + k_2)} \left(\frac{m_1\Lambda}{2T}\right)^{-2b} \ln\left(\frac{m_2\Lambda}{2T}\right)^2
$$

$$
- \frac{R_b^{01}(k_1)R_b^{11}(k_2)}{(\varepsilon + \frac{1}{2}n - b + q/2 + k_1 + k_2)^2} \left(\frac{m_1\Lambda}{2T}\right)^{-2b}
$$

$$
+ \frac{R_b^{01}(k_1)R_b^{01}(k_2)}{(\varepsilon + \frac{1}{2}n - 2b + q/2 + k_1 + k_2)} \left(\frac{m_1\Lambda}{2T}\right)^{-2b} \left(\frac{m_2\Lambda}{2T}\right)^{-2b} \Bigg]. \tag{2.7}
$$

The r.h.s. of (2.7) has to be considered in the limit for $\Lambda \to \infty$ and details about the angular expansion coefficient $A_0^0(q)$ and the radial expansion coefficients $R_b^{00}(k)$, $R_b^{01}(k)$ and $R_b^{11}(k)$ are given in [1].

Possible infinities are found as a denominator factor, caused by the close to zero x integration, and it is seen that if

$$
\tfrac{1}{2}n - 2b > 0, \tag{2.8}
$$

all terms in the summations of (2.7) are finite. In four dimensional space $(n = 4)$, the last term gives an infinity for $\frac{1}{2}q = k_1 = k_2 = 0$. Due to the exponentially decreasing character of the integrand of the r.h.s. of (2.1), the sum of the remaining summations converges in the limit $\Lambda \to \infty$,

$$
(2.7) = \frac{\pi^2}{\varepsilon} + \text{finite terms}. \tag{2.9}
$$

Compared with the Feynman parameter method, this way of computing Feynman diagrams is circumstantial in the case of Figure 6, but the method has advantages

when applied on diagrams with overlapping divergences. The latter are mixed together by the Feynman parameters, but well separated in configuration space.

In [1], the formalism has been extended to a general scalar Feynman diagram with I internal lines with masses m_{0i}, m_{ij} $(1 \le i < j \le V-1)$, V vertices and L loops. By counting the orders of the functions $k_b(mx)$ in the integrand, it is found that infinities, caused by near zero x-integrations, occur if

$$\tfrac{1}{2}n(V-1) - Ib \le 0. \tag{2.10a}$$

Counting of loops and internal lines in momentum space yields

$$nL - 2I \tag{2.10b}$$

as degree of divergence. (2.10b) is in agreement with (2.10a) because of the equality $L + V = I + 1$, and the degree of divergence of a scalar Feynman diagram is $-2 \times$ l.h.s. (2.10a).

Introduction of spin leads to momenta in the numerator. The expressions of the two-vertex vector diagrams of Figure 7 are

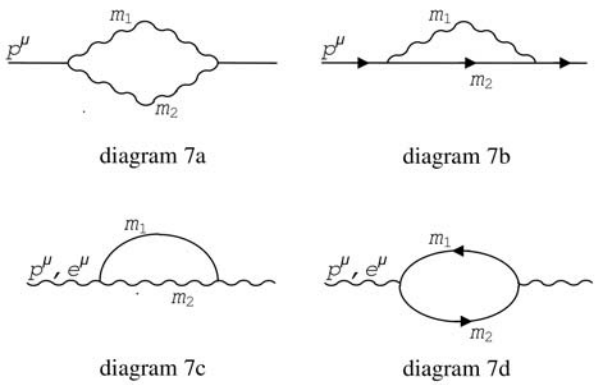

Figure 7. Two-vertex diagrams with vector lines.

$$\text{diagram 7a/b/c/d} = \int d^n k_1 d^n k_2 \delta^n(p - k_1 - k_2) \frac{T_{\text{a/b/c/d}}}{({k_1}^2 + {m_1}^2)({k_2}^2 + {m_2}^2)} \tag{2.11}$$

with

$$T_{\text{a}} = \frac{(k_{1\mu}k_{1\nu} + {m_1}^2 g_{\mu\nu})({k_2}^\mu {k_2}^\nu + {m_2}^2 g^{\mu\nu})}{{m_1}^2 {m_2}^2}, \tag{2.12a}$$

$$T_{\rm b} = \frac{(k_{1\mu}k_{1\nu} + {m_1}^2 g_{\mu\nu})\overline{w}\gamma^{\mu}(\gamma.k_2 + m_2)\gamma^{\nu}w}{{m_1}^2}, \tag{2.12b}$$

$$T_{\rm c} = \frac{(e.k_1)^2 + {m_1}^2}{{m_1}^2}, \tag{2.12c}$$

$$T_{\rm d} = {\rm Tr}\{\gamma.e(\gamma.k_1 + m_1)\gamma.e(\gamma.k_2 + m_2)\}. \tag{2.12d}$$

Momenta in the numerator correspond to derivatives of the k_b - functions and each derivative ∂_x lowers the denominator factor of the corresponding expansion by $\frac{1}{2}$. Hence, infinities are found if

$$\tfrac{1}{2}n(V-1) - bI - B - [\tfrac{1}{2}F] \le 0, \tag{2.13}$$

in which B is the number of internal boson lines, F is the number of internal fermion lines and $[\frac{1}{2}F]$ is the integer of $\frac{1}{2}F$ and the degree of divergence is at most $-2 \times$ l.h.s. (2.13). Thus, the diagrams of Figure 7 seem to be quartic, cubic, quadratic and quadratic, respectively and they seemingly result into a non-renormalizable theory.

However, momentum conservation, which means substitution of

$$k_1.k_2 = \tfrac{1}{2}\{{k_1}^2 + {k_2}^2 - (k_1 - k_2)^2\} \tag{2.14a}$$

into (2.12a) and substitution of

$$k_1^{\mu} = p^{\mu} - k_2^{\mu} \tag{2.14b}$$

into (2.12b) and into (2.12d), reduces the number of derivatives, since $(k_1 - k_2)^2$ is the square of an external mass and also the internal momentum squares ${k_1}^2$ and ${k_2}^2$, though off the mass shell, become squares of masses when using the differential equation (2.4). Nor the r.h.s. of (2.14b) causes a raise in the number of derivatives because of the equality $(\gamma.k_2)^2 = {k_2}^2$, which becomes a mass square as well. Thus, the configuration space expressions become

$$(2.12a) = \frac{(2\pi^{n/2})^2(m_1m_2)^{2b}}{(2\pi)^n}\left\{\frac{({m_1}^2 + {m_2}^2 - p^2)^2}{4{m_1}^2{m_2}^2} + n - 2\right\}$$

$$\times \int d^n x e^{ip.x} k_b(m_1 x) k_b(m_2 x), \tag{2.15a}$$

$$(2.12b) = \frac{(2\pi^{n/2})^2 (m_1 m_2)^{2b}}{(2\pi)^n}$$

$$\times \int dx e^{ip.x} \begin{bmatrix} \frac{1}{2} i(m_1^2 + m_2^2 - p^2) \overline{w}\gamma.\hat{x} w x k_{b+1}(m_1 x) k_b(m_2 x) \\ + \frac{1}{2} i m_2^2 (n-3) \overline{w}\gamma.\hat{x} w x k_b(m_1 x) k_{b+1}(m_2 x) \\ + (n-1) m_2 \overline{w} w k_b(m_1 x) k_b(m_2 x) \end{bmatrix}, \tag{2.15b}$$

$$(2.12c) = \frac{(2\pi^{n/2})^2 (m_1 m_2)^{2b}}{(2\pi)^n} \int d^n x e^{ip.x}$$

$$\times \left[\{1 + (e.\hat{x})^2\} k_b(m_1 x) - \tfrac{1}{2} \{1 - n(e.\hat{x})^2\} k_{b+1}(m_1 x) \right] k_b(m_2 x), \tag{2.15c}$$

$$(2.12d) = \frac{(2\pi^{n/2})^2 (m_1 m_2)^{2b}}{(2\pi)^n} 2^{[n/2]} \int d^n x e^{ip.x}$$

$$\times \left\{ -\tfrac{1}{2} m_1^2 m_2^2 (e.\hat{x})^2 \; x^2 k_{b+1}(m_1 x) k_{b+1}(m_2 x) \right.$$

$$\left. + \tfrac{1}{2} (m_1^2 + m_2^2 - p^2 \; + 2n m_1 m_2) k_b(m_1 x) k_b(m_2 x) \right\} \tag{2.15d}$$

and, considering the sum of the orders of the k_b-functions minus the power of x^2 in the integrand, the reduced degrees of divergence are found to be logarithmic, logarithmic, quadratic and quadratic, respectively, which is less strong than indicated by (2.13).

Relations of momenta correspond to relations of derivatives in configuration space. Therefore, the relations (2.14), above demonstrated in the case of diagrams with two external lines, remain valid if all three lines of a vertex are internal, i.e., off the mass shell. Thus, reduction of the degree of divergence happens in any diagram of spinning fields and the divergence criterion (2.13) may be replaced by the less severe criterion

$$(V-1)\tfrac{1}{2} n - bI - B_{nn} + \tfrac{1}{2} V_{FV} - [\tfrac{1}{2} F] \leq 0, \tag{2.16}$$

in which B_{nn} is the number of non-neighbouring internal vector lines, V_{FV} is the number of vertices of an internal vector and two spinors. The degree of divergence becomes at most $-2 \times$ l.h.s. (2.16).

3. Possible Diagrams and their Divergences

Because of our restriction of the possible vertices according to the Figures 1 and 2, the structure of a general Feynman diagram, resulting from the Lagrangian (1.1), is restricted. It consists of a number of loops of spinors and vectors. A spinor or vector loop may be open, i.e., starting and ending as external lines, or closed. Moreover, an open vector loop may start or end at a spinor. Furthermore, spinor lines may be interconnected by a number of vectors and vector lines may be interconnected by a number of scalars. Scalar lines may be interconnected by scalars through φ^4 or φ^3 vertices. Examples of possible two-, three- and four-vertex diagrams are drawn in the Figures 8-10.

Higher order diagrams may be considered as obtained from lower order by insertion of internal lines or closed loops. In this way, diagrams of Figure 8 are obtained from those of Figure 7.

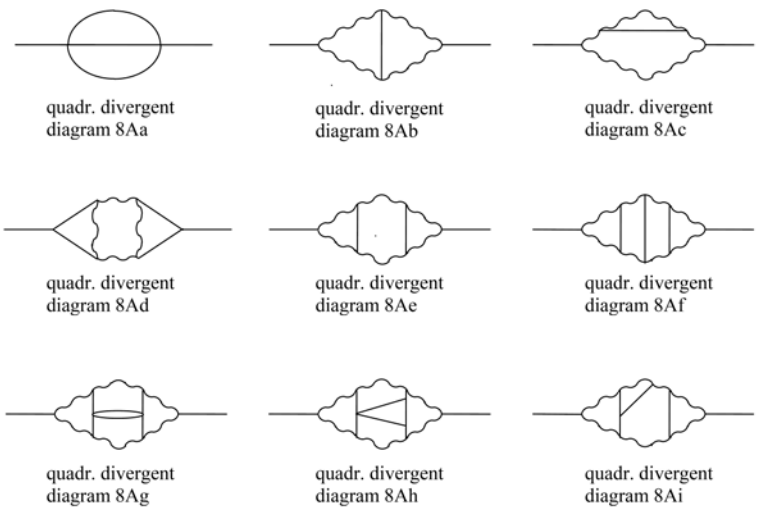

Figure 8A. Two external scalars.

Figure 8B. Two external spinors.

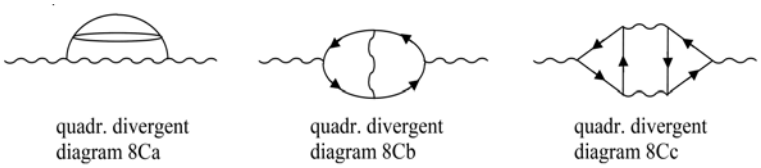

Figure 8C. Two external vectors.

In all these cases, the increase of V, I, B_{nn} and $[\frac{1}{2}F]$, caused by the insertion of an internal line, may be considered and it is seen that the l.h.s. of (2.16) either remains unchanged or decreases. An exception is diagram 7a, which is logarithmic divergent whereas insertion of lines leads to the quadratically divergent diagrams 8Ab, 8Ac, 8Ae and 8Af. Another exception is the diagram 10Ca. Insertion of a scalar lowers the degree of divergence by two, but it is raised by two after insertion of a second internal scalar. The general behaviour, also in cases of exception, is that insertion of lines or loops does not lead to a higher degree of divergence.

Since the degree of divergence does not increase in higher orders, it may be concluded that:

(a) divergences of diagrams with two external lines (Figure 8) are at most quadratic and, therefore, their infinity may be removed by counter terms of the kind $\partial_\mu\varphi\partial^\mu\varphi$, $\partial_\mu W_\nu\partial^\mu W^\nu$, $i\overline{\psi}\partial^\mu\psi$, φ^2, $W_\mu W^\mu$, $\overline{\psi}\psi$;

(b) divergences of diagrams with three external lines (Figure 9) are at most logarithmic and, therefore, their infinity may be removed by counter terms of the kind φ^3, $W_\mu W^\mu\varphi$, and $\overline{\psi}\gamma^\mu\psi W_\mu$;

(c) divergences of diagrams with four external scalars (Figure 10A) are at most logarithmic and a divergence may be removed by a counter term of the kind φ^4;

(d) diagrams with four external spinors, diagrams with two external spinors and vectors and diagrams with two external spinors and scalars (Figure 10B) are finite;

(e) diagrams with more than four external lines are finite.

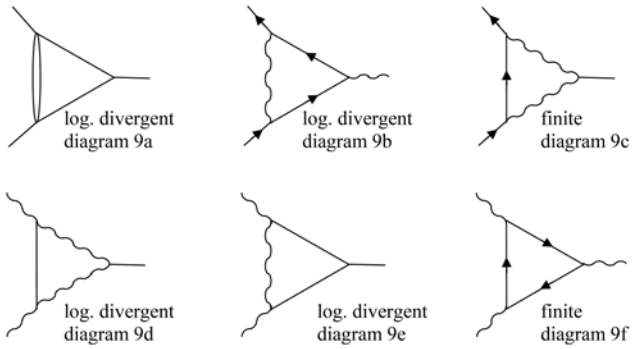

Figure 9. Three external lines.

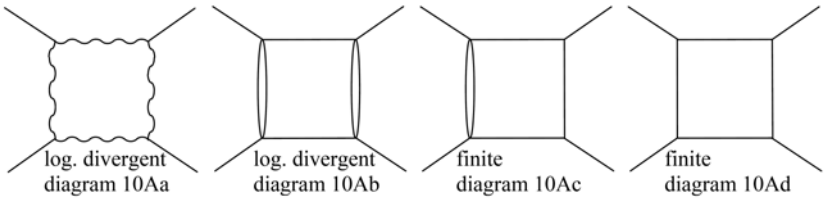

Figure 10A. Four external scalars.

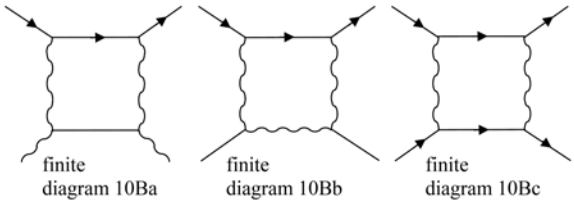

Figure 10B. Four-vertex diagrams with external spinors.

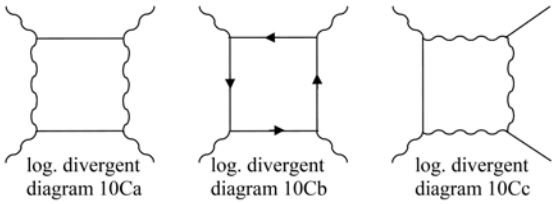

Figure 10C. Four-vertex diagrams with external vectors.

Diagrams with four external vectors and diagrams with two external vectors and scalars (Figure 10C) are logarithmically divergent. The removal of these infinities by

counter terms, which would be of the kind $(W_\mu W^\mu)^2$ and $W_\mu W^\mu \varphi^2$, causes new and stronger divergences and the situation would transit from bad to worse. This way has not been chosen in [1] and will not be chosen in this paper. Instead, relations are imposed on the coupling constants in such a way that their divergences disappear. This is possible because of the fact that the divergence of all diagrams with four external lines is at most logarithmic.

4. Non-renormalizibility of Tensor-scalar Interactions

In this section, the method of the preceding section is applied on the Lagrangian (1.3), where a tensor field $W^{\mu\nu}$ has been added to the model. Using the propagator (1.5), it is seen that the expressions for the two-vertex diagrams of Figure 11 are

$$\text{diagram 11a/b/c/d} = \int d^n k_1 d^n k_2 \delta^n (p - k_1 - k_2) \times \frac{T_{\text{a/b/c/d}}}{(k_1^2 + m_1^2)(k_2^2 + m_2^2)} \tag{4.1}$$

with

$$T_{\text{a}} = \frac{(k_{1\mu} k_{1\nu} k_{1\rho} k_{1\sigma} + m_1^2 k_{1\mu} k_{1\rho} g_{\nu\sigma} + m_1^2 k_{1\mu} k_{1\sigma} g_{\nu\rho} + m_1^4 g_{\mu\rho} g_{\nu\sigma}) \times (k_2^\mu k_2^\nu k_2^\rho k_2^\sigma + m_2^2 k_2^\mu k_2^\rho g^{\nu\sigma} + m_2^2 k_2^\mu k_2^\sigma g^{\nu\rho} + m_2^4 g^{\mu\rho} g^{\nu\sigma})}{m_1^4 m_2^4}, \tag{4.2a}$$

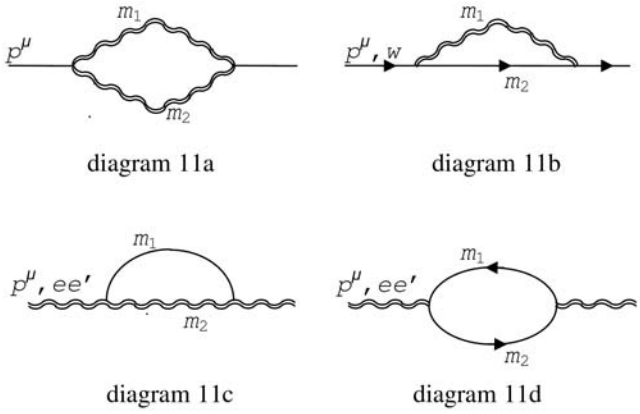

Figure 11. Two-vertex diagrams with tensor lines.

$$T_b = \frac{\begin{array}{l}(k_{1\mu}k_{1\nu}k_{1\rho}k_{1\sigma} + {m_1}^2 k_{1\mu}k_{1\rho}g_{\nu\sigma} + {m_1}^2 k_{1\mu}k_{1\sigma}g_{\nu\rho} \\ + {m_1}^4 g_{\mu\rho}g_{\nu\sigma})\overline{w}\gamma^{\mu\nu}(\gamma.k_2 + m_2)\gamma^{\rho\sigma}w\end{array}}{{m_1}^4}, \tag{4.2b}$$

$$T_c = \frac{\begin{array}{l}e_\mu e'_\nu e_\rho e'_\sigma({k_2}^\mu {k_2}^\nu {k_2}^\rho {k_2}^\sigma + {m_2}^2 {k_2}^\mu {k_2}^\rho g^{\nu\sigma} \\ + {m_2}^2 {k_2}^\mu {k_2}^\sigma g^{\nu\rho} + {m_2}^4 g^{\mu\rho}g^{\nu\sigma})\end{array}}{{m_1}^4}, \tag{4.2c}$$

$$T_d = e_\mu e'_\nu e_\rho e'_\sigma \,\mathrm{Tr}\{\gamma^\mu\gamma^\nu(\gamma.k_1 + m_1)\gamma^\rho\gamma^\sigma(\gamma.k_2 + m_2)\}. \tag{4.2d}$$

Since more momenta are present in the numerator of the tensor propagator (1.5), diagrams with internal tensor lines are stronger divergent than the corresponding vector diagrams but, as in the vector case, many of these momenta may be transformed into mass dependent factors by the relations (2.14) and (2.4). Using the relations of Appendix E of [1], the configuration space expressions of the diagrams of Figure 11 become

$$(4.2a) = \left\{ n(n-2) + \frac{({m_1}^2 + {m_2}^2 - p^2)^4 + 8(n-1){m_1}^2{m_2}^2({m_1}^2 + {m_2}^2 - p^2)^2}{16{m_1}^4{m_2}^4} \right\}$$

$$\times \frac{(2\pi^{n/2})^2(m_1m_2)^{2b}}{(2\pi)^n}\int d^n x e^{ip.x} k_b(m_1x)k_b(m_2x), \tag{4.3a}$$

$$(4.2b) = \frac{(2\pi^{n/2})^2(m_1m_2)^{2b}}{(2\pi)^n}\int d^n x e^{ip.x}$$

$$\times\Big[\tfrac{1}{2}\, i(n-1)(n-5){m_2}^2\overline{w}\gamma.\hat{x}wxk_b(m_1x)k_{b+1}(m_2x)$$

$$-(n-1)^2 m_2\overline{w}wk_b(m_1x)k_b(m_2x)\Big], \tag{4.3b}$$

$$(4.2c) = \frac{(2\pi^{n/2})^2(m_1m_2)^{2b}}{(2\pi)^n}\int d^n x e^{ip.x}k_b(m_1x)$$

$$\times\Big[\Big\{1 + (e.\hat{x}e'.\hat{x})^2 - e.e'e.\hat{x}e'.\hat{x} - (e.\hat{x})^2\Big\}k_b(m_2x)$$

$$+\tfrac{1}{2}\Big\{2(n+2)(e.\hat{x}e'.\hat{x})^2 - (e'.\hat{x})^2 - (n+1)(e.\hat{x})^2 + (e.e')^2 - (n+4)e.e'e.\hat{x}e'.\hat{x}$$

$$+1\ \Big\}k_{b+1}(m_2x)+\tfrac{1}{4}\Big\{(n+2)(n+4)(e.\hat{x}e'.\hat{x})^2\ -4(n+2)e.e'e.\hat{x}e'.\hat{x}$$

$$-(n+2)(e'.\hat{x})^2-(n+2)(e.\hat{x})^2\ +2(e.e')^2+1\Big\}k_{b+2}(m_2x)\Big], \qquad (4.3c)$$

$$(4.2d)=\frac{(2\pi^{n/2})^2(m_1m_2)^{2b}}{(2\pi)^n}\,2^{[n/2]}\int d^n x e^{ip.x}$$

$$\times\Big[\Big\{-\tfrac{1}{2}(2e.e'^2-1)(m_1{}^2+m_2{}^2-p^2\ )+m_1m_2(2e.e'-1)\Big\}k_b(m_1x)k_b(m_2x)$$

$$-\tfrac{1}{2}(m_1m_2)^2\Big(e.\hat{x}^2\ +e'.\hat{x}^2-2e.e'e.\hat{x}e'.\hat{x}\Big)x^2k_{b+1}(m_1x)k_{b+1}(m_2x)\Big]. \qquad (4.3d)$$

From the close to zero behaviour of the integrand of these expressions, it may be seen that the degrees of divergence of the expressions (4.3) are logarithmic, logarithmic, quartic and quadratic, respectively.

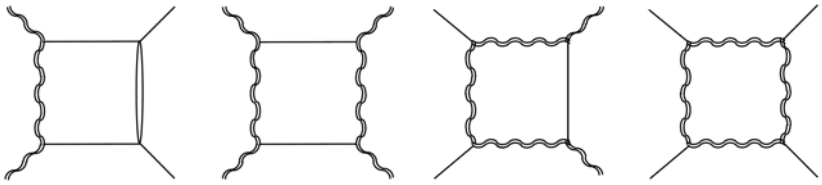

Figure 12. Four-vertex tensor-scalar diagrams.

In the same way, the tensor-scalar diagrams of Figure 12, are seen to be quadratic or quartic divergent.

The divergence of some of the diagrams of Figures 11 and 12 still are too strong to be renormalizable, despite the reduction by means of the relations (2.14) and (2.4).

5. Cancellation of Divergences

Because of the latter conclusion, tensor-scalar vertices are excluded and interactions of the tensor field with only spinor fields are allowed, so that diagrams like 11a, 11c and those of Figure 12 do not occur. Therefore, we consider the Lagrangian (1.8), describing g fermion fields, interacting with a tensor and a vector field. The vector field is interacting with a self interacting scalar field, a tensor-scalar

interaction term is omitted. Under these conditions, internal tensor lines only occur between two spinors and the momenta in the numerator are transformed by (2.14b) into momenta in traces of spinors or between the external $\overline{w}$ and w. Using the formalism of Section 2, they become squares of masses. In this way, the momenta in the numerator of the tensor propagator do not raise the degree of divergence, the venom-teethes of internal tensor lines are extracted and the divergence criterion (2.16) remains valid.

In the way of Section 2:

• the divergences of a diagram with two external tensors are quadratic or logarithmic and may be compensated by counter terms of the kind $\partial_\rho W_{\mu\nu}\partial^\rho W^{\mu\nu}$ and $W_{\mu\nu}W^{\mu\nu}$;

• the divergence of diagrams with two external spinors and one external tensor is logarithmic and may be compensated by counter terms of the kind $\overline{\psi}_f \gamma_\mu \gamma_\nu \psi_f W^{\mu\nu}$.

Moreover, counting the number of $\gamma.e$'s and $\gamma.k$'s of the fermion loop, it may be seen that:

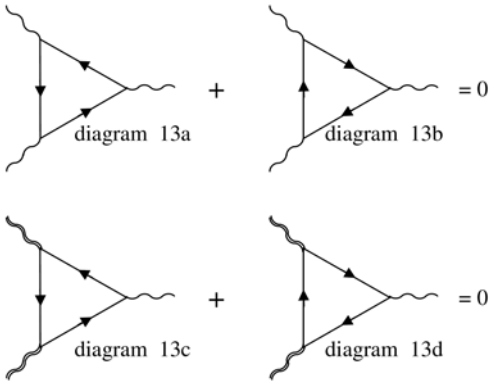

Figure 13. One-loop diagrams with three internal spinors and an odd number of external vectors.

• the two diagrams 13a and 13b with three external vectors and one (anti-)loop of three fermions are cancelling each other, which is Furry's theorem [7] in lowest order; the cancellation is also found if two external vectors are replaced by tensors, like in the diagrams 13c and 13d;

• in Figure 14, where one or three vectors of Figure 13 are replaced by tensors, the contributions of loop and anti-loop are equal, so they do not cancel, but the diagrams are finite since the number F of internal fermions is odd.

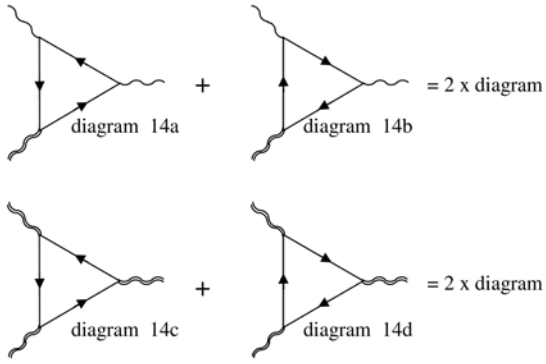

Figure 14. One-loop diagrams with three internal spinors and an odd number of external tensors.

In the case of diagrams with one (anti-)loop of four spinors, it is the other way around:

• the divergence of all diagrams of Figures 15 and 16 is logarithmic, as argued in the beginning of this section.

• the diagrams of Figure 15 with an odd number of external tensors and vectors are cancelling;

• the diagrams of Figure 16 with an even number of external tensors and vectors are equal, so they are not mutually cancelling;

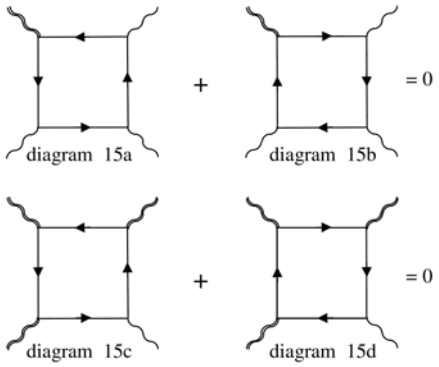

Figure 15. One-loop diagrams with an even number of internal spinors and an odd number of external tensors.

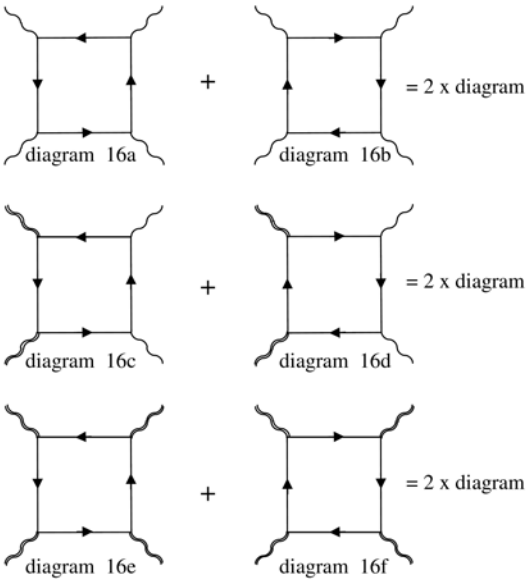

Figure 16. One-loop diagrams with an even number of internal spinors and an even number of external tensors.

The above points are clear in the cases of the demonstrated lower order diagrams and are proven in higher order by induction, in the way of Section 3.

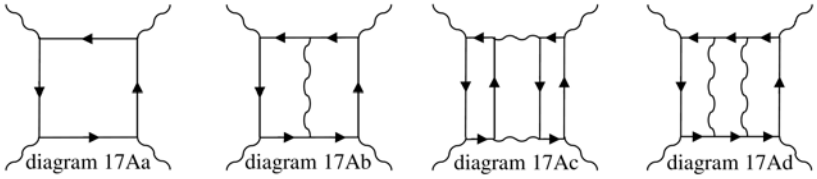

+ similar and higher order diagrams + internal wave lines replaced by double wave lines + arrow lines replaced by double arrow lines.

Figure 17A. Four external vectors.

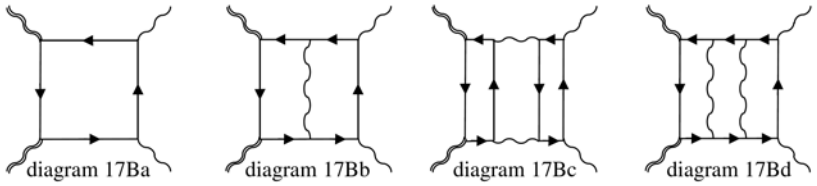

+ similar and higher order diagrams + internal wave lines replaced by double wave lines + arrow lines replaced by double arrow lines.

Figure 17B. Two external tensors, two external vectors.

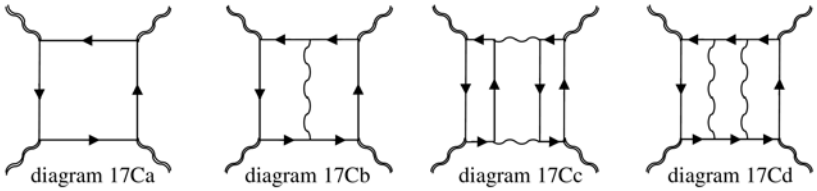

+ similar and higher order diagrams + internal wave lines replaced by double wave lines + arrow lines replaced by double arrow lines.

Figure 17C. Four external tensors.

The removal of the divergence from all these diagrams by counter terms, which would be of the kind $(W_\mu W^\mu)^2$ and $(W_{\mu\nu} W^{\mu\nu})^2$, causes new and stronger divergences.

However, we choose the way out that also has been followed in the vector case. Due to the fact that the divergence of the diagrams of Figure 17 is not stronger than logarithmic, to all orders of perturbation, the scattering matrix, which is the sum of these diagrams multiplied by a pre-factor, becomes finite (not each diagram apart) if the coupling constants satisfy the equations

$$\lim_{\varepsilon\to 0} \varepsilon \left\{ \sum_{q} \frac{\lambda_{FT}^{V_{FT}} \lambda_{FV}^{V_{FV}} \lambda_{VS}^{V_{VS}} \lambda_{S}^{V_S} (-)^{L_F} \times (\text{diagram } 17\text{Jq})}{(2\pi)^{\frac{3}{2}E+4(L-1)}} \right\} = 0 \qquad (5.1)$$

with J = A, B, C.

If there is only one fermion field and no vector-scalar interaction $(g = 1, \lambda_{VS} = 0)$ there are three equations for two coupling constants, which is too much. The most simple Lagrangian allowing a solution of the latter equations is that of two fermion fields, without tensor-scalar and vector-scalar interaction $(g = 2, \lambda_{TS} = \lambda_{VS} = 0)$, i.e., with only spinor-tensor and spinor-vector vertices, as drawn in Figure 4. In this way, the four coupling constants belonging to the vertices of Figure 4 are restricted by the three relations (5.1) and it is possible to construct a finite scattering matrix, order by order in a perturbation approach.

Secondly, the case $g = 2$ and one scalar field interacting with the vector field, is considered. The vertices are those of Figures 1 and 4. They lead to the diagrams of Figure 17, complemented by diagrams with vector-scalar interactions, and to those of Figure 18. In this way, there are six coupling constants (presence of φ^3 vertices

leads to finite diagrams), restricted by the three relations (5.1) and by the two relations

$$\lim_{\varepsilon\to 0}\varepsilon\left\{\sum_{q}\frac{\lambda_{FT}{}^{V_{FT}}\lambda_{FV}{}^{V_{FV}}\lambda_{VS}{}^{V_{VS}}\lambda_{S}{}^{V_{S}}(-)^{L_F}\times(\text{diagram 18Jq})}{(2\pi)^{\frac{3}{2}E+4(L-1)}}\right\}=0 \qquad (5.2)$$

with J = A, B

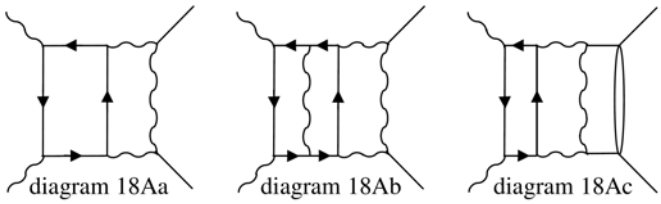

+ similar and higher order diagrams + internal wave lines replaced by double wave lines + arrow loops replaced by double arrow loops.

Figure 18A. Two external vectors and scalars.

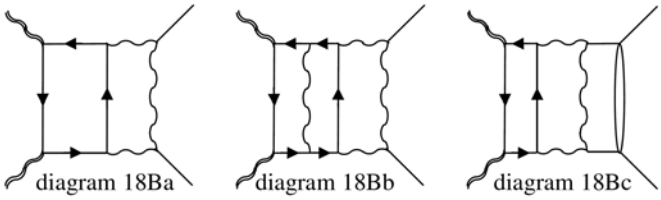

+ similar and higher order diagrams + internal wave lines replaced by double wave lines + arrow loops replaced by double arrow loops.

Figure 18B. Two external tensors and scalars.

and in this case too, it is possible to construct a finite scattering matrix, order by order in a perturbation approach.

6. Conclusion

A unitary model of massive tensors and vectors in interaction with spinors and scalars, leading to a finite scattering matrix, is possible in the case of two spinor fields with direct spinor-tensor and spinor-vector interactions. Vector-scalar interaction is possible, but not necessary. Tensor-scalar interaction is excluded.

Divergences of diagrams with two and three external lines may be removed by counter terms in the Lagrangian. Diagrams with four external lines have a

divergence, which is at most logarithmic, and can only be removed by a counter term in the case of four external scalars. In all other cases of four external lines, a finite scattering matrix may be constructed, order by order in perturbation, by relations between coupling constants.

The formalism is massive, and massless fields may be described in our model by considering the limit of a small tensor mass. Self-interactions of the tensor field are excluded. The latter may be approached by considering the diagrams of Figures 13-18 in the limit of large masses of the intermediate spinor loops.

The formalism is covariant under global, but not under local Lorentz transformations. In this way, non-renormalizable divergences, as found in the locally gauge invariant formalism [8-10], are avoided.

Acknowledgement

The author thanks Mrs. C. W. Israëls-Perlstein for linguistic improvements.

References

[1] E. Mendels, Ann. Phys. 325 (2010), 2307.

[2] F. Englert and R. Brout, Phys. Rev. Lett. 13 (1964), 321.

[3] P. W. Higgs, Phys. Rev. Lett. 13 (1964), 508.

[4] G. S. Gouralnic, C. R. Hagen and T. W. B. Kibble, Phys. Rev. Lett. 13 (1964), 585.

[5] G. ‘t Hooft, Nucl. Phys. B35 (1971), 167.

[6] G. N. Watson, A Treatise on the Theory of Bessel Functions, Cambridge University Press, Cambridge, 1935.

[7] W. H. Furry, Phys. Rev. 51 (1937), 125.

[8] G. 't Hooft and M. Veltman, Annales Poincaré Phys. Theor. A20 (1974), 69.

[9] M. H. Goroff and A. Sagnotti, Phys. Lett. B160 (1985), 81.

[10] M. H. Goroff and A. Sagnotti, Nucl. Phys. B266 (1986), 709.